Theoretical predictions of red and near-infrared strongly emitting *X*-annulated rylenes

Qian Peng,[1] Yingli Niu,[1] Zhaohui Wang,[1] Yuqian Jiang,[2] Yan Li,[1] Yajun Liu,[3] and Zhigang Shuai[1,2,a)]

[1]*Key Laboratory of Organic Solids, Beijing National Laboratory for Molecular Science (BNLMS), Institute of Chemistry, Chinese Academy of Sciences, Beijing 100190, People's Republic of China*
[2]*Key Laboratory of Organic OptoElectronics and Molecular Engineering, Department of Chemistry, Tsinghua University, Beijing 100084, People's Republic of China*
[3]*College of Chemistry, Beijing Normal University, Beijing 100875, People's Republic of China*

(Received 2 September 2010; accepted 7 January 2011; published online 18 February 2011)

The optical properties of rylenes are extremely interesting because their emission colors can be tuned from blue to near-infrared by simply elongating the chain length. However, for conjugated chains, the dipole-allowed odd-parity $1B_u$ excited state often lies above the dipole-forbidden even-parity $2A_g$ state as the chain length increases, thus preventing any significant luminescence according to Kasha's rule. We systemically investigated the $1B_u/2A_g$ crossover behaviors with respect to the elongating rylene chain length with various quantum chemistry approaches, such as time-depended density functional theory (TDDFT), complete active space self-consistent field theory (CASSCF/CASPT2), multireference configuration interaction (MRCI)/Zerner's intermediate neglect of diatomic overlap (ZINDO), and MRCI/modified neglect of differential overlap. The calculated results by CASSCF/CASPT2 and MRCI/ZINDO are completely coherent: the optical active $1B_u$ state lies below the dark B_{3g} or $2A_g$ state for perylene and terrylene, which results in strong fluorescence; while a crossover to $S_1 = 2A_g$ occurs and leads to much weaker fluorescence for quaterrylene. Then we put forward a molecular design rule on how to recover fluorescence for the longer rylenes by introducing heteroatom bridges. Several heteroatom-annulated rylenes are designed theoretically, which are predicted to be strongly emissive in the red and near-infrared ranges. These are further confirmed by theoretical emission spectra as well as radiative and nonradiative decay rate calculations by using the vibration correlation function formalisms we developed earlier coupled with TDDFT. © *2011 American Institute of Physics*. [doi:10.1063/1.3549143]

I. INTRODUCTION

The conjugated luminescent oligomers and polymers with low band gap are highly desired for applications such as optical communication,[1] photodetector,[2] solar cell,[3] and chemical/biological sensors.[4] Rylenes have a backbone consisting of perilinked naphthalene units [Fig. 1(a)]. The optical properties of oligorylenes are extremely interesting because their emission colors can be tuned from blue to near-infrared by elongating the chain length.[5] However, the emission quantum yields of perylene and terrylene are very high and close to unity,[6–8] while those of quaterrylene and longer rylenes are very small.[9] This is really a nasty problem in the design of efficient luminescent red and infrared materials. Therefore, it is highly desired to study the luminescent mechanism of rylenes from first principles and it is also of great interest to functionalize long rylenes for the strong red and infrared emission.

The two key requirements for highly efficient luminescent materials are: (i) the strongly dipole-allowed transition from the lowest excited singlet state (S_1) to the ground state (S_0) according to Kasha's rule, which has been widely applied to the luminescent conjugated materials[10] and (ii) the high molecular fluorescent quantum yield, which is determined by the competition between the radiative decay and the nonradiative decay from S_1 to S_0.[11]

As to the first requirement, we mainly focus on the low-lying excited electronic states orderings for the compounds. The $1B_u/2A_g$ crossover behaviors in the conjugated systems such as polyene, diphenylpolyene, and polyyne have been intensely studied both experimentally and theoretically in the past.[12,13] The lowest-lying state S_1 being the 2^1A_g state instead of the optically active $1B_u$ in diphenyloctatetrace was discovered by Hudson and Kohler.[14] The first theoretical analysis was made by Schulten and Karplus.[15] They ascribed the ordering anomaly to the electron correlation effects. Since then, there have been continuous and considerable investigations, such as by Tavan and Schulten,[16] Cave and Davidson,[17] Nakayama *et al.*,[18] Hsu *et al.*,[19] Serrano-Andres *et al.*,[20] Starcke *et al.*,[21] Marion and Gilka,[22] Shahi *et al.*,[23] in calculating the $2A_g/1B_u$ orderings for the short unsubstituted polyene and Shukla[24] for the substituted polyene [poly(diphenylacetylene)]. It is found that the $2A_g$ state has important contributions from electron double excitation configuration in the molecular orbital picture. The nearly exact solution based on the density matrix renormalization group theory have been successfully obtained for understanding the crossover behavior for very long chain

a)Author to whom correspondence should be addressed. Electronic mail: zgshuai@tsinghua.edu.cn.

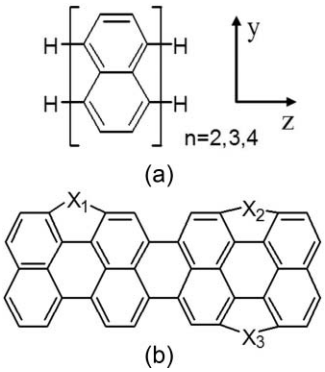

FIG. 1. Molecular structures of (a) rylenes and (b) heteroatom *X*-annulated quaterrylene: $X_1 = X_2 = N$, *N*, *N*, *N*-annulated quaterrylene (QNN); $X_1 = S$, $X_2 = N$, *N*, *S*-annulated quaterrylene (QNS); $X_1 = X_3 = N$, NQN; $X_1 = N$, $X_3 = S$, NQS.

(80 -π-electrons) by Shuai *et al.*[25] and Barford *et al.*[26] Does similar situation occur in rylenes? Experimentally, in Ref. 9, Koch and Müllen presented the absorption and emission spectra of perylene, terryelene, and quaterrylene in 1, 4-dioxane, and there always is a nice "mirror image" character in the absorption and emission spectra for the three oligorylens, which indicates that the fluorescence and absorption are originated from the same dipole-allowed electronic state. However, in helium buffer gas, Deperasińska *et al.* found the indication of a dark electronic state below the dipole-allowed electronic state for jet-cooled terrylene.[27] The experimental findings indicate, for oligorylenes, subjected to the environment, that the orderings of the excited states could be changed. Theoretically Karabunarliev *et al.* studied the oligorylenes by using different semiempirical and concluded that for quaterrylene, the optically opaque state becomes the lowest excited state adiabatically, not vertically, while for shorter rylenes, the lowest excited states are dipole-allowed both adiabatically and vertically.[28–30] Therefore, there certainly occurs a $1Bu/2A_g$ crossover when elongating oligorylenes length, and terrylene and quaterrylene may be both close to the crossover point.

In this work, we first compare the different quantum chemistry methods for the excited state orderings from the perylene, terrylene to quaterrylene, including time-depended density functional theory (TDDFT), multireference configuration interaction (MRCI) based on semiempirical Hamiltonian, and a second-order perturbation on top of complete active space self-consistent field theory (CASPT2). We found that only the CASPT2 and MRCI/Zerner's intermediate neglect of diatomic overlap (ZINDO) methods can give reliable results. Then we use the MRCI/ZINDO method to calculate a series of extended *X*-annulated rylenes in order to search the light-emitting molecules (S_1 to be dipole-allowed). A recent effort based on synthesizing *N*-annulated rylenes compounds has shown great promise for red light emission.[31] The overall trend is fully consistent with the simple rule we proposed earlier,[32] on how to make the chemical substitution effective for light emitting based on the molecular orbital calculations. The main idea arises from the fact that $1B_u$ state is an ionic excitation and consists of mostly the highest occupied molecular orbital (HOMO) to lowest unoccupied molecular orbital (LUMO) single excitation. For a molecule with $2A_g$ state lying below $1B_u$, if the chemical substitution can induce appreciable charge modification at the frontier orbitals HOMO and LUMO, the $1B_u$ state can thus be stabilized, as a result, it becomes the lowest excited state, thus allowing light-emission. In our previous work,[32] we have shown that some substituted polyacetylenes are nonemissive while some others are strongly emissive. However, for the substituted polydiacetylene, it is impossible to make it light-emitting by such a side-chain substitution. These theoretical calculations have rationalized the experimental findings. In order to further extend the emission wavelength, we elongate the chain up to tetra-*N*-annulated octerylene (84 heavy atoms). We predict it to be light-emitting based on molecular orbital calculations only and the emitting wavelength is around 1008 nm from TDDFT calculation.

Once the optically allowed state becomes the lowest, considering the second requirement for the highly efficient luminescent materials, it is necessary to examine the molecular fluorescent quantum yield, that is, by comparing the radiative decay and nonradiative decay rates from S_1 to S_0. Here, for the screened strongly dipole-allowed luminescent molecules, we calculate the spectra, radiative and nonradiative decay rates by the vibration correlation function formalism we developed earlier.[33] Using such formalism, we have previously rationalized the exotic aggregation induced emission phenomenon in several molecules.[34] We have also studied the effect of polyene chain length on the photophysical properties in diphenylpolyenes,[35] and we have analyzed the emission spectra for the luminescent group-14 metalloles.[36]

This paper is organized as follows: (i) after this Introduction, we will describe the computational techniques for the excited states as well as the formalism of the optical spectra and excited state decay rates; (ii) then we will present the results on the excited state orderings for rylenes and heteroatom annulated rylenes, along with the molecular orbital analysis for the heteroatom bridges' effects; (iii) and finally, we will describe the emission spectra and excited state decays rates for the selected light-emitting molecules.

II. THEORETICAL METHODOLOGY AND COMPUTATIONAL TECHNIQUES

A. Excited state structure calculations

Excited state remains a major challenge for quantum chemistry. For small molecules, the state-of-the-art methods are complete active space self-consistent field theory (CASSCF/CASPT2) and couple-cluster equation of motion (EOM-CC) or equivalently linear response. While for the larger system, the most popular method is TDDFT. As has been shown before, TDDFT fails to describe the correct excited state orderings,[37] and the $2A_g$ state is often calculated to be above $1B_u$. In the wavefunction description, $2A_g$ is of multireference character. However, if the lowest excited state is truly $1B_u$, the TDDFT can be applied both efficiently and satisfactorily. For many organic molecules, the semiempirical

methods have been quite successful in describing the excited structure and can be applied to much larger molecules than the *ab initio*. In fact, Hutchison, Ratner, and Marks[38] have compared the experimental results of optical absorption with many computational methods for a group of 60 common conjugated molecules and they found that mean absolute deviation for TDDFT is comparable with that of the semiempirical ZINDO, and both can reproduce reasonably well the excited state values.

Thus, in this work, for the excited state structure calculations, we have employed and compared the *ab initio*, semiempirical, and TDDFT methods. With density functional theory (DFT), we optimize the S_0 geometries for all the compounds studied in this work (see Fig. 1), and evaluate the vibration frequencies and normal modes by analytical second-order derivatives. The TDDFT is first applied to calculate the vertical excitation energies for the four lowest-lying excited states at the optimized S_0 geometries for oligorylenes, and then to optimize the S_1 geometry and compute the vibration frequencies and normal modes by numerical differentiation of the analytical energy gradients for perylene, terrylene, and the heteroatom-annulated rylenes. The B3LYP and BLYP functionals[39] are applied. The DFT/TDDFT calculations are carried out in the TURBOMOLE 6.0 program package.[40] In the semiempirical approach, the molecular vertical excitation energies of the four low-lying excited states at S_0 geometry in oligorylenes are calculated by using multireference configuration interaction with single and double excitations within the modified neglect of differential overlap (MNDO)[41] Hamiltonian (MRCI/MNDO) as implemented by Lei *et al.*[42] and the multireference determinant single and double interactions[43] coupled with the ZINDO Hamiltonian[44] (MRCI/ZINDO), which has been greatly expanded by us in terms of both active space and the number of configurations. For the *ab initio* side, we employed the second-order perturbation method based on the CASSCF/CASPT2 as implemented in the MOLCAS 6.4 package.[45] The active space is 12 electrons in 12 π orbitals. For quaterrylene, the frozen orbitals are adapted on the 1s orbitals of carbon. The multistate CASPT2[46] is used to calculate the vertical excitation energies.

In the MRCI/MNDO calculations, CI orbital space includes all the adjacent occupied and unoccupied π orbitals. The reference states are defined as the complete active space, and cas(8, 8) is used, namely, eight active electrons in eight π orbitals. In the MRCI/ZINDO calculations, for molecules perylene and terrylene, the active space includes all the adjacent occupied and unoccupied π orbitals, and at most 12 occupied and 12 unoccupied molecular orbitals are included for larger molecules. To construct the configuration space, we choose the six important reference configurations, including the Hartree-Fock ground state, three single-excitation configurations (HOMO $\rightarrow$ LUMO, HOMO – 1 $\rightarrow$ LUMO, and HOMO $\rightarrow$ LUMO + 1), and two double-excitation configuration (HOMO, HOMO $\rightarrow$ LUMO, LUMO and HOMO – 1, HOMO $\rightarrow$ LUMO, LUMO + 1).

For the first-principles calculations, the 6–31G* basis set is used and the D_{2h}, C_{2v}, C_{2h}, C_s point groups are adapted for the oligorylenes and the heteroatom-annulated rylene derivatives, respectively, when the geometries in S_0 are optimized. There are no symmetry restraints for the optimization of geometries in S_1.

Once a molecule is predicted to be of light-emitting, the emission spectra and the radiative and radiativeless decay rates are calculated by means of a vibration correlation function program developed in our group, which considers the displaced and distorted Duschinsky rotation effect as well as the Herzberg–Teller effect for the multimode harmonic oscillators.

B. Absorption and emission spectroscopy

The absorption cross section $\sigma_{\rm abs}(\omega, T)$ defined as the rate of photon energy absorption per molecule and per unit radiant energy flux, is given by the explicit expression with dimensions of $\rm cm^2$:[33,47,48]

$$\sigma_{\rm abs}(\omega, T) = \frac{4\pi^2\omega}{3c}\sum_{v_i,v_f} P_{iv_i}(T)|\langle\Theta_{fv_f}|\vec{\mu}_{fi}|\Theta_{iv_i}\rangle|^2 \times\delta(\hbar\omega - E_{fi} - E_{fv_f} + E_{iv_i}). \quad (1)$$

Similarly, the emission spectrum $\sigma_{\rm em}(\omega, T)$ defined as the rate of spontaneous photon emission per molecule and per unit frequency between ω and $\omega + {\rm d}\omega$, is given as the dimensionless differential spontaneous photon emission rate $\rm cm^2$:[33,47,48]

$$\sigma_{\rm em}(\omega, T) = \frac{4\omega^3}{3c^3}\sum_{v_i,v_f} P_{iv_i}(T)|\langle\Theta_{fv_f}|\vec{\mu}_{fi}|\Theta_{iv_i}\rangle|^2 \times \delta(E_{if} + E_{iv_i} - E_{fv_f} - \hbar\omega). \quad (2)$$

Here ω represents the vibration frequency. c is the velocity of light in vacuum. $P_{iv_i}(T)$ is the Boltzmann distribution function for the initial vibronic manifold at finite temperature T. $\vec{\mu}_{fi} = \langle\Phi_f|\vec{\mu}|\Phi_i\rangle$ is the electric transition dipole moment between two electronic states $|\Phi_i\rangle$ and $|\Phi_f\rangle$. $|\Theta_{iv_i}\rangle$ and $|\Theta_{fv_f}\rangle$ are the vibrational states. $E_{if} = E_i - E_f$ represents the adiabatic excitation energy. $E_{iv_i} = \sum_k E_{iv_{ik}}$ and $E_{fv_f} = \sum_k E_{fv_{fk}}$ are the total vibrational energy of the molecule in the initial and final electronic states, respectively.

In general, $\vec{\mu}_{fi}$ depends on the nuclear coordinate, and can be expanded in the normal coordinates as

$$\vec{\mu}_{fi} = \vec{\mu}_0 + \sum_k \vec{\mu}_k Q_k + \sum_{k,l} \vec{\mu}_{kl} Q_k Q_l + \cdots. \quad (3)$$

For the strongly dipole-allowed transitions, the spectrum is usually dominated by the zero-order term $\vec{\mu}_0$ [Franck–Condon (FC) approximation]. While for the weakly dipole-allowed or dipole-forbidden transitions, the Herzberg–Teller approximation corresponding to the first-order term (HT approximation) should be considered.

Applying the Fourier transformation, $\delta(\omega) = 1/2\pi \int e^{i\omega t} dt$, Eq. (1) can be written as

$$\sigma_{\rm abs}(\omega, T) = \sigma^{\rm FC}_{{\rm abs},0}(\omega, T) + \sum_k \sigma^{\rm FC/HT}_{{\rm abs},k}(\omega, T) + \sum_{k,l} \sigma^{\rm HT}_{{\rm abs},kl}(\omega, T). \quad (4)$$

Here

$$\sigma_{\rm abs}^{\rm FC}(\omega,T)=\frac{2\pi\omega}{3\hbar c}\int e^{i\omega t}e^{-iE_{fi}t/\hbar}Z_{iv}^{-1}\rho_{\rm abs,0}^{\rm FC}(t,T)\mathrm{d}t, \tag{5}$$

$$\sigma_{\rm abs}^{\rm FC/HT}(\omega,T)=\frac{2\pi\omega}{3\hbar c}\vec{\mu}_0\cdot\vec{\mu}_k \times\int e^{i\omega t}e^{-iE_{fi}t/\hbar}Z_{iv}^{-1}\rho_{{\rm abs},k}^{\rm FC/HT}(t,T)\mathrm{d}t, \tag{6}$$

$$\sigma_{\rm abs}^{\rm HT}(\omega,T)=\frac{2\pi\omega}{3\hbar c}\vec{\mu}_k\cdot\vec{\mu}_l \times\int e^{i\omega t}e^{-iE_{fi}t/\hbar}Z_{iv}^{-1}\rho_{{\rm abs},kl}^{\rm HT}(t,T)\mathrm{d}t, \tag{7}$$

and

$$\rho_{\rm abs,0}^{\rm FC}(t,T)=\mathrm{Tr}[e^{-i\tau_f\hat{H}_f}e^{-i\tau_i\hat{H}_i}], \tag{8}$$

$$\rho_{{\rm abs},k}^{\rm FC/HT}(t,T)=\mathrm{Tr}\left[Q_{fk}e^{-i\tau_f\hat{H}_f}e^{-i\tau_i\hat{H}_i}\right], \tag{9}$$

$$\rho_{{\rm abs},kl}^{\rm HT}(t,T)=\mathrm{Tr}\left[Q_{fk}e^{-i\tau_f\hat{H}_f}Q_{fl}e^{-i\tau_i\hat{H}_i}\right], \tag{10}$$

are the three kinds of thermal vibration correlation function of the absorption spectrum.

In order to get the fully analytical formalism of Eq. (4), the path integral formula of harmonic oscillator is adopted to derive the integrals.[49,50]

We further define

$$\tilde{\mu}_{\rm abs}^2(t,T)=|\vec{\mu}_0|^2-\sum_k\vec{\mu}_0\cdot\vec{\mu}_k\left[\underline{H}_k^{\rm FC/HT}\mathbf{K}^{-1}\underline{F}\right]+\sum_{kl}\vec{\mu}_k\cdot\vec{\mu}_l \times\left[i\hbar\mathrm{Tr}\left[\mathbf{G}_{kl}^{\rm HT}\mathbf{K}^{-1}\right]+(\mathbf{K}^{-1})^T\mathbf{G}_{kl}^{\rm HT}(\mathbf{K}^{-1})\right], \tag{11}$$

then the final analytic solution of the correlation function can be expressed as

$$\sigma_{\rm abs}(\omega)=\frac{2\pi\omega}{3\hbar c}\int e^{i(\omega-\omega_{fi})t}Z_{iv}^{-1}\rho_{\rm abs,0}^{\rm FC}(t,T)\,\tilde{\mu}_{\rm abs}^2(t,T)\,\mathrm{d}t, \tag{12}$$

where

$$\rho_{\rm abs,0}^{\rm FC}(t,T)=\sqrt{\frac{\det\left[\mathbf{a}_f\mathbf{a}_i\right]}{\det\left[\mathbf{K}\right]}} \times\exp\left\{-\frac{i}{\hbar}\left[\frac{1}{2}\underline{F}^T\mathbf{K}\underline{F}-\underline{D}^T\mathbf{E}\underline{D}\right]\right\}. \tag{13}$$

On the other hand, the emission spectrum $\sigma_{\rm em}(\omega,T)$ has the similar form:

$$\sigma_{\rm em}(\omega)=\frac{2\omega^3}{3\pi\hbar c^3} \times\int e^{-i(\omega-\omega_{if})t}Z_{iv}^{-1}\rho_{\rm em,0}^{\rm FC}(t,T)\,\tilde{\mu}_{\rm em}^2(t,T)\,\mathrm{d}t, \tag{14}$$

where $\mathbf{a}_i$, $\mathbf{a}_f$, and $\mathbf{E}$ are the $N\times N$ matrices, $\mathbf{G}$ and $\mathbf{K}$ are the $2N\times 2N$ matrices, D is the $N\times 1$ column matrix, F and H are the $2N\times 1$ column matrices, respectively. The more details of the correlation function are given in Ref. 33.

C. Radiative and nonradiative decay rate

1. Radiative decay rate

The radiative decay rate, i.e., the spontaneous emission rate, is simply the integration of the light emission spectrum:

$$k_{\rm r}=\int_0^\infty\sigma_{\rm em}(\omega)\,d\omega \tag{15}$$

2. Internal conversion rate

According to Fermi's golden rule, the nonradiative internal conversion rate can be expressed as

$$k_{\rm ic}=\frac{2\pi}{\hbar}\left|H'_{fi}\right|^2\delta\left(E_{fi}+E_{fv_f}-E_{iv_i}\right). \tag{16}$$

Here the perturbation is the non-Born–Oppenheimer coupling:

$$H'_{fi}=-\hbar^2\sum_l\left\langle\Phi_f\Theta_{fv_f}\left|\frac{\partial\Phi_i}{\partial Q_{fl}}\frac{\partial\Theta_{iv_i}}{\partial Q_{fl}}\right\rangle\right. . \tag{17}$$

Applying the Condon approximation, Eq. (17) becomes

$$H'_{fi}=\sum_l\langle\Phi_f|\hat{P}_{fl}|\Phi_i\rangle\langle\Theta_{fv_f}|\hat{P}_{fl}|\Theta_{iv_i}\rangle, \tag{18}$$

where $\hat{P}_{fl}$ is the normal momentum operator.

Inserting (18) into (16), the IC rate can be expressed as

$$k_{\rm ic}=\sum_{kl}k_{{\rm ic},kl}, \tag{19}$$

where

$$k_{{\rm ic},kl}=\frac{2\pi}{\hbar}R_{kl}Z_{iv}^{-1}\sum_{v_i,v_f}e^{-\beta E_{iv_i}}P_{kl}\delta(E_{fi}+E_{fv_f}-E_{iv_i}) \tag{20}$$

and

$$R_{kl}=\langle\Phi_f|\hat{P}_{fk}|\Phi_i\rangle\langle\Phi_i|\hat{P}_{fl}|\Phi_f\rangle, \tag{21}$$

$$P_{kl}=\langle\Theta_{fv_f}|\hat{P}_{fk}|\Theta_{iv_i}\rangle\langle\Theta_{iv_i}|\hat{P}_{fl}|\Theta_{fv_f}\rangle. \tag{22}$$

The delta function is Fourier transformed as

$$k_{{\rm ic},kl}=\frac{1}{\hbar^2}R_{kl}\int_{-\infty}^{\infty}\mathrm{d}t\left[e^{i\omega_{if}t}Z_{iv}^{-1}\rho_{{\rm ic},kl}(t,T)\right], \tag{23}$$

where $\rho_{{\rm ic},kl}(t,T)$ is the IC correlation function,

$$\rho_{{\rm ic},kl}(t,T)=\mathrm{Tr}\left[\hat{P}_{fk}e^{-i\tau_f\hat{H}_f}\hat{P}_{fl}e^{-i\tau_i\hat{H}_i}\right]. \tag{24}$$

The final form of the IC correlation function is

$$\rho_{{\rm ic},kl}(t,T)=\sqrt{\frac{\det[\mathbf{a}_f\mathbf{a}_i]}{\det[\mathbf{K}]}}\exp\left\{-\frac{i}{\hbar}\left[\frac{1}{2}\underline{F}^{\rm T}\mathbf{K}^{-1}\underline{F}-\underline{D}^{\rm T}\mathbf{E}\underline{D}\right]\right\} \cdot\left\{i\hbar\mathrm{Tr}\left[\mathbf{G}_{kl}^{\rm IC}\mathbf{K}^{-1}\right]+(\mathbf{K}^{-1}\underline{F}^{\rm T})\mathbf{G}_{kl}^{\rm IC}(\mathbf{K}^{-1}\underline{F}) -\left(\underline{H}_{kl}^{\rm IC}\right)^{\rm T}\mathbf{K}^{-1}\underline{F}\right\} \tag{25}$$

TABLE I. Vertical excitation energies (eV) of the four low-lying excited states at the ground state geometry for the oligorylenes. The oscillator strengths of the dipole-allowed states are given in the parenthesis.

	TDDFT						
	B3LYP	BLYP	CASSCF	CASPT2	MRCI/MNDO	MRCI/ZINDO	Ref. 28
Perylene	B_{1u}: 2.86 (0.3616)	B_{1u}: 2.55 (0.2682)	B_{3g}: 4.44	B_{1u}: 3.24 (0.5644)	B_{3g}: 2.68	B_{1u}:3.42 (0.5997)	3.337
	B_{3g}: 3.65	B_{3g}: 3.29	B_{1u}: 4.46	B_{3g}: 3.38	B_{2u}: 2.68	B_{3g}: 3.65	
	B_{3g}: 4.03	B_{3g}: 3.27	B_{2u}: 4.62	A_g: 3.74	B_{1u}: 2.88	A_g: 4.16	
	B_{2u}: 4.00	A_g: 3.60	A_g: 4.79	B_{2u}: 3.77	A_g: 2.90	B_{2u}: 4.74	
Terrylene	B_{1u}: 2.21 (0.7557)	B_{1u}: 2.00 (0.6314)	B_{1u}: 3.41	B_{1u}: 2.62 (1.2274)	B_{1u}:2.55	B_{1u}: 2.92 (1.0984)	2.774
	A_g: 3.10	A_g: 2.55	B_{2u}: 3.64	A_g: 2.75	A_g: 2.80	Ag: 3.06	3.252
	B_{3g}: 3.29	B_{3g}: 2.85	A_g: 3.75	B_{3g}: 3.51	B_{2u}: 3.45	Ag: 4.24	
	B_{2u}: 3.30	B_{2u}: 2.90	B_{3g}: 4.63	B_{2u}: 3.86	B_{2u}: 3.47	B_{2u}: 4.69	
Quaterrylene	B_{1u}: 1.83 (1.2271)	B_{1u}: 1.66 (1.0559)	B_{1u}: 2.74	A_g:1.99	B_{1u}: 2.28	Ag: 2.49	2.807
	A_g: 2.46	A_g: 1.96	A_g: 3.01	B_{1u} :2.01 (1.3092)	Ag:2.59	B_{1u}: 2.53 (1.5501)	2.454
	A_g: 2.90	B_{3g}: 2.50	B_{1u}: 3.89	B_{3g}: 2.93	B_{1u}: 2.52	B_{3g}: 3.48	
	B_{3g}:2.92	A_g: 2.65	B_{3g}: 4.21	A_g: 2.96	B_{3g}: 4.05	Ag: 3.99	

Comparing the IC correlation function Eq. (25) with the FC correlation function Eq. (13), we find that these formalisms have the very similar mathematic structure. The more details of the correlation function are also given in Ref. 33. All the quantities that appeared in these formulae are computed by either DFT or TDDFT.

III. RESULTS AND DISCUSSIONS

A. Vertical excitation energies of oligorylenes

Starting from the optimized ground-state geometries by using B3LYP/6–31G*, the vertical excitation energies of the four low-lying excited states for perylene, terrylene, and quaterrylene are calculated using TDDFT, MRCI/MNDO, MRCI/ZINDO, and CASSCF/CASPT2 methods, respectively, and the results are collected in Table I. In the meantime, the oscillator strengths for the dipole-allowed excited states and the previously calculated values[28] are also included in Table I. The dominant electronic configurations describing the excited states of the compounds and their weights in the CASSCF wave function are summarized in Table II. In addition, the wavefunction in the atomic orbital representation of the HOMO and of the LUMO are shown in Fig. 2.

From Table I, it is obvious that the CASPT2 and MRCI/ZINDO give very similar results for the four lowest excited states in the oligorylenes. Especially for the two lowest excited states, the two methods show completely coherent results: the dipole-allowed B_{1u} state lies below the dipole-forbidden B_{3g} (or 2Ag) and $2A_g$ state for perylene and terrylene, respectively, which leads to strong luminescence, while a crossover to $S_1 = 2A_g$ happens for quaterrylene, which results in weak fluorescence. Results also indicate that the allowed transition dipole moment is along the long chain orientation z-axis. The results are distinctly different from those calculated by resorting to the CASSCF and MRCI/MNDO and the pervious calculation based on the semiempirical PM3 model as given in Ref. 29. This indicates that (i) the perturbation correction is necessary at the level of CASSCF for the oligorylenes; (ii) ZINDO parameters are appropriate for describing the excitations in oligorylenes, however the other semiempirical methods are not specifically parametrized for spectroscopy. Sometimes, the semiempirical methods overestimate the σ–π correlation and artificially lower the covalent states, leading to the false ordering of electronic states[51,18]

In addition, TDDFT/B3LYP (or BLYP) is qualitatively wrong in describing such ordering, as the $2A_g$ excited state mostly consists of double excitations from HOMO to LUMO in conjunction with two single ones from HOMO–1 to LUMO and from HOMO to LUMO + 1 (see Table II). As mentioned above, at the present stage, TDDFT/B3LYP (or BLYP) is unable to describe the excited state with double excitation character, since only singly excited states are contained in the linear response formalism[52] and the errors in the excitation energies for these states can be as large as a few eV.[37] Nevertheless, it is very useful when the lowest excited state is indeed an odd-parity $1B_u$ state.

It is important to note that the MRCI/ZINDO method is both reliable and efficient, as have been extensively shown previously.[43,53] Most importantly, comparing to CASPT2, it can be applied to much larger molecules, which offers us an efficient tool for designing light-emitting molecules.

From Fig. 2, it can be seen that for the three oligorylenes, the HOMO is always of the a_u symmetry and the LUMO is of the b_{1g} symmetry. The two a_u and b_{1g} orbitals are both odd with respect to the σ_z and σ_y mirror planes, but are odd and even with respect to the σ_z mirror plane, respectively. Accordingly, the orbitals are disjointed, with the conjugation

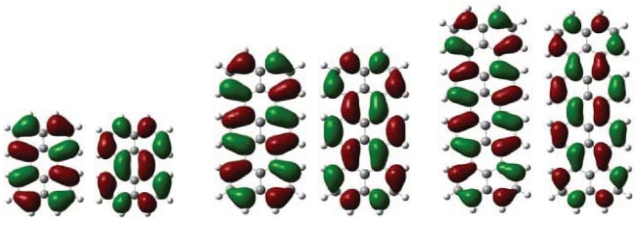

FIG. 2. The atomic orbital composition of selected molecular orbitals in perylene, terrylene, and quaterrylene at the B3LYP/6–31G*level.

TABLE II. The main configurations in CASSCF wave function of the two low-lying states of oligorylenes. The orbital symmetry, and the selected weight (>0.10) in the wave function are given.

Molecules	Elec. States	Wave functions	
Perylene	B_{1u}	Single excitation: HOMO (a_u) → LUMO (b_{1g})	0.84
	B_{3g}	Single excitation: HOMO-1 (b_{2g}) → LUMO (b_{1g})	0.27
		Single excitation: HOMO (a_u) → LUMO + 1 (b_{3u})	0.38
Terrylene	B_{1u}	Single excitation: HOMO (a_u) → LUMO (b_{1g})	0.88
	$2A_g$	Double excitation: HOMO (a_u) → LUMO (b_{1g})	0.44
		Single excitation: HOMO (a_u) → LUMO + 1 (a_u)	0.19
		Single excitation: HOMO – 1 (b_{1g}) → LUMO (b_{1g})	0.19
Quaterrylene	$2A_g$	Double excitation: HOMO (a_u) → LUMO (b_{1g})	0.43
		Single excitation: HOMO (a_u) → LUMO + 1 (a_u)	0.15
		Single excitation: HOMO – 1 (b_{1g}) → LUMO (b_{1g})	0.17
	B_{1u}	Single excitation: HOMO (a_u)→ LUMO (b_{1g})	0.89

running along the two peripheral *trans–cis* C=C chains. Thus an oligorylene can be decomposed into two polyene chains. As shown in Ref. 54, in the case of parallel ordering, there is no mixing between the valence and conduction bands of different chains and the system is more like a two-independent-chain system. Therefore, an oligorylene with n naphthalene units is comparable with a polyene chain with $2n$ double bonds. However, the electron correlation in oligorylenes is less substantial,[55] and there are many configurations involving the other molecular orbitals except the frontier molecular orbitals. Therefore, unlike polyenes, a crossover from $S_1 = 1B_u$ to $S_1 = 2A_g$ occurs in quaterrylene whose conjugation length corresponds to eight C=C coupled bonds.

B. Design of heteroatom-annulated quaterrylene derivatives

It has been well understood that the fundamental mechanism for the lowest excited state crossover from odd-parity to even-parity is the electron correlation effect. Odd-parity state (emissive) is the ionic excitation, while the even-parity (dark) is the covalent or spin-flipping excitation. Chen *et al.*[32] have shown that side-chain substitution can significantly modify the charge distribution at the frontier orbitals, thus can induce an excited state ordering swapping, namely, the lowest-lying state is stabilized from even-parity to odd-parity, thus allowing light-emission. They defined a quantity $\rho_{H/L}$ as follows:

$$\rho_{H/L} = \frac{\sum_\kappa |C_{H_\kappa}|^2}{\sum_\kappa |C_{L_\kappa}|^2}, \tag{26}$$

where $C_{H(L)}$ is the molecular orbital coefficient of the HOMO (LUMO) at the backbone site κ at which substituent moieties (heteroatom in this work) are linked to. If $\rho_{H/L}$ is close to 1, the substitution contributes equally to HOMO and LUMO, thus does not modify appreciably the charge character for the ionic $1B_u$ state, as the $1B_u$ consists mainly of a transition from HOMO to LUMO. Therefore, it is expected that if $\rho_{H/L}$ is close to 1, the substitution does not cause alternation in the ordering of $1B_u$ vs $2A_g$. However, if $\rho_{H/L}$ is well away from 1, either much larger than or much less than 1, the $1B_u$ state can be stabilized as the lowest excited state. This speculation has been confirmed by the excited state structure calculations at the highly accurate EOM-CC level as well as by experimental evidences for the substituted polyacetylenes and polydiacetylenes.[32]

In order to make the long oligorylenes emissive, we introduce the heteroatom bridges in the backbone [Fig. 1(b)]. The $\rho_{H/L}$ values calculated with B3LYP/6–31g* for the *X*-annulated quaterrylene QNN, NQN, QNS, and NQS are 2.54, 2.30, 1.85, and 1.70, respectively, which are deviated appreciably from 1. From the HOMO and LUMO orbitals of the four compounds plotted in Fig. 3, it can be seen that the heteroatoms indeed induce charge redistribution in the frontier orbitals, that is, heteroatoms do not appear in the HOMO wavefunction but are present in the LUMO wavefunction.

We then calculated the vertical excitation energies and the oscillator strengths for the two lowest-lying excited states by using MRCI/ZINDO (Fig. 4). There is an obvious $1B_u/2A_g$ crossover from quaterrylene to the *X*-annulated ones. The orientations of the allowed transition dipole moment (with large oscillator strength) in *X*-annulated quaterrylene compounds are the same as those of oligorylens, that is, along the chain orientation *z*-axis.

C. Photophysical properties

For these luminescent compounds with dipole-allowed transition from S_1 to S_0, we further optimized the geometries of S_1 and calculated the vibration frequencies and the normal mode coordinates in the S_1 and S_0 states. The transition electric fields for each atom at the ground equilibrium geometry for the compounds are calculated at the TDDFT/B3LYP /6–31G* level by using the GAUSSIAN 03 program package[56] in order to calculate the electronic coupling terms for the

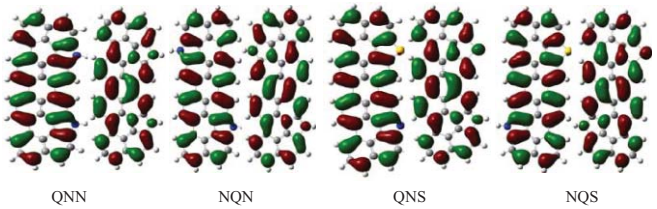

FIG. 3. B3LYP/6–31g* HOMO (left) and LUMO (right) orbitals.

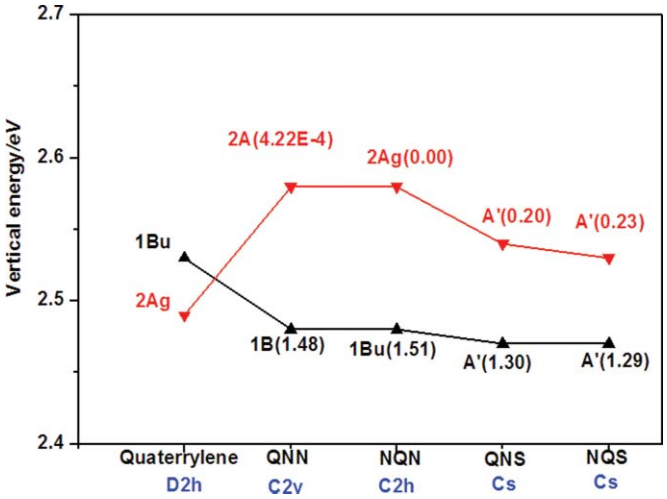

FIG. 4. The low-lying excited states of quaterrylene and the *X*-annulated quaterrylene calculated by using the MRCI/ZINDO. The transition oscillator strengths are given in parenthesis, and the point groups are shown for the molecules at the ground state at the bottom.

internal conversion nonradiative rate, more details are given in Ref. 33. Finally, based on the electronic structure information the spectra and the radiative and nonradiative decay rates are calculated.

1. Absorption and emission spectra

We compare the theoretical absorption and emission spectra for perylene with the well-established experimental measures. The calculated vertical excitation energy from the S_0 ($1A_g$) to S_1 ($1B_u$) is 2.90 eV, which is close to the previously calculated results by using TDDFT, and smaller than the previously calculated ones, 3.337 (Ref. 6) or 3.018 eV and the adiabatic excited energy (2.70 eV) is in good agreement with the experimental result 2.86 eV,[57] somewhat lower than the previous theoretical values, 2.98 Ref. 58 and 3.146 eV.[6]

Comparison of the calculated absorption spectrum at $T = 20$ K with the experimental measurement[59] is shown in Fig. 5(a). The absorption spectrum is broadened by the Lorentzian function with a full width at half maximum (FWHM) of 10 cm^{-1}. The excited state is optimized by using the TDDFT/B3LYP method. TDDFT/B3LYP underestimates the excitation energy by 0.35 eV. Based on the optimized geometry, we calculated the vibronic couplings for all the normal modes with the excited state. Duschinsky rotation and Herzberg–Teller effects are both taken into account. We shift the origin of the theoretical spectrum so that the 0–0 transitions coincide. It can be seen that the line shapes of the calculated spectrum, which stem from the coupling between the electronic excited state and the vibration mode, agree excellently with the experiment. This validates the vibration correlation function theory and the electronic structure method adapted in this work.

The calculated emission spectra with the same Lorentzian function constant FWHM = 10 cm^{-1} at T = 20 and 300 K are reported in Fig. 5(b). In the emission spectra, the dominated peak is the 0–0 transition, and the

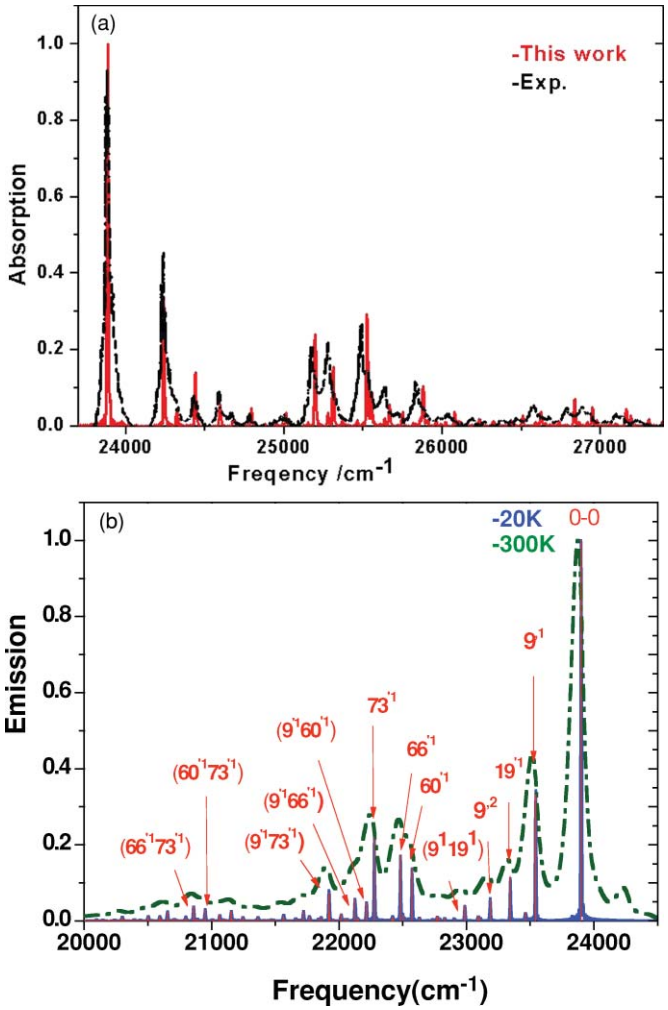

FIG. 5. (a) The absorption spectra at $T = 20$ K of perylene (solid for the calculated spectrum and dash dot for the experimental one); (b) the emission spectra of perylene (solid line for the $T = 20$ K, dash dot for $T = 300$ K) and their assignments of transition (vertical lines) which are labeled as N^{ν} (N is the index of the excited normal modes and ν is the quantum number).

other peaks with high vibration states are labeled as N^{ν}(N is the index of the excited normal modes and ν is the quantum number). The involved normal modes and the corresponding frequencies in the spectra progressions are given in Fig. 6. The lowest frequency of Franck–Condon active vibrations, the longitudinal stretching motion of the whole molecule, is 357 cm^{-1}, which is consistent with the experimental observation value (near 350 cm^{-1});[60] the mode 19 is the transverse stretching motion of the whole molecule; the mode 60 is the vibration related to the C–C bonds linking two naphthalene

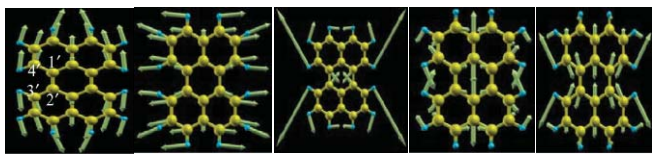

FIG. 6. The dominant normal modes involved in the emission spectra for perylene. The corresponding frequencies of normal modes are shown in parentheses.

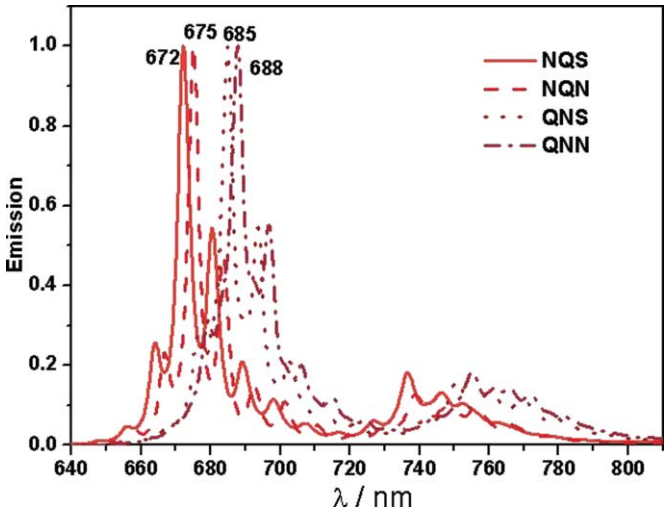

FIG. 7. Theoretical emission spectra for the *X*-annulated quaterrylene derivatives at $T = 300$ K.

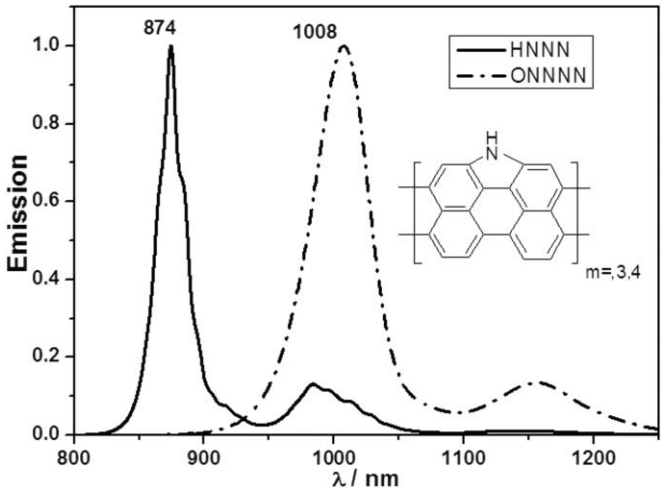

FIG. 8. Theoretical emission spectra for *tri-N*-annulated hexarylene (HNNN) and tetra-*N*-annulated octerylene (ONNNN). The sizes are beyond capability of the present quantum chemistry methods, which can be used to predict their excited state structures. We thus resort to the molecular orbital calculations according to Eq. (19). The $\rho_{H/L}$ values are calculated to be 2.46 and 2.45, respectively. Thus, we predict that these two compounds are emissive. At the same time, the predicted emission spectra are given in Fig. 8, where the maximum emission peaks are at 874 and 1008 nm, respectively.

units; the mode 66 is the breathing mode; and the mode 73 is the C–C bond stretching parallel to the central axis. These results are also in good agreement with the previous calculations,[7] and moreover, the frequency values are more close to the values in Raman scattering.[61] In addition, the transition features are consistent with the changed features of geometry from the excited state. The changes mainly localize on the C1–C4, C2–C3, C1′–C4′, C2′–C3′, C1–C2, and C1′–C2′ bonds (the labels can be seen in Fig. 6), and their values are 0.0332, 0.0332, 0.0332, 0.0332, –0.0321, and –0.0321 Å, respectively.

The calculated emission spectra for *X*-annulated quaterrylenes are depicted in Fig. 7. The maximum peak positions are at 672, 675, 685, and 688 nm for NQS, NQN, QNS, and QNN, respectively. The computed value 688 nm of QNN is in good agreement with the available experimental 694 nm[31] of the similar compound, which add two naphthalene rings to both ends and two alkyl chains to two nitrogen atoms. The active modes involved in the emission process are assigned and the frequencies of the modes are showed in Table III. The modes mainly relate to the stretching motions of C–C bonds, similar to the corresponding ones in perylene. For the longer conjugated systems, the modes are always softened, that is, the frequencies become smaller. The main changes of geometry upon excitation also localize on the C–C bonds of the central perylene in the four *X*-annulated quaterrylenes, similar to the ones in perylene.

We further increase the *N*-annulated perylene unit, to *tri-N*-annulated hexarylene (HNNN) and tetra-*N*-annulated octerylene (ONNNN). The sizes are beyond capability of the present quantum chemistry methods, which can be used to predict their excited state structures. We thus resort to the molecular orbital calculations according to Eq. (19). The $\rho_{H/L}$ values are calculated to be 2.46 and 2.45, respectively. Thus, we predict that these two compounds are emissive. At the same time, the predicted emission spectra are given in Fig. 8, where the maximum emission peaks are at 874 and 1008 nm, respectively.

TABLE III. The frequencies of active modes involved in the emission process for the *X*-annulated quaterrylene derivatives.

Molecules	Frequencies (cm^{-1})
NQS	183, 547, 567, 1300, 1414, 1587
NQN	185, 554, 1300, 1415, 1581
QNS	97, 184, 547, 1306, 1404, 1571
QNN	100, 189, 553, 1297, 1414, 1584

2. Nonradiative and radiative decay rates

Nonradiative rate from the first excited state is generally the sum of the internal conversion rate from S_1 to S_0 (k_{ic}) and the intersystem crossing rate from S_1 to T_1 (k_{isc}). The phosphorescence emission is expected to be very weak,[62] even not detectable[45] in perylene, and there is no observable transition to triplet state in terrylene.[63] Thus the k_{isc} is very small and can be neglected. Therefore, we will focus on the internal conversion rates k_{ic} and compare them with the radiation rates k_r for the oligorylenes and *X*-annulated rylene derivatives.

The calculated radiative and nonradiative decay rates from S_1 to S_0 for the compounds are presented in Table IV. From Table IV, it can be seen that the calculated results can well reproduce the available experimental observations, that is, there exists very high fluorescent quantum yields in perylene and terrylene. With the elongated conjugated chain, the

TABLE IV. The calculated radiative and nonradiative transition rates from S_1 to S_0 rates for the oligorylenes and the *X*-annulated rylene derivatives.

Molecules	$k_r/(s^{-1})$	k_{ic} (s^{-1})
Perylene	0.91E + 08	0.72E + 03
Terrylene	0.12E + 09	0.51E + 05
NQS	0.15E + 09	0.25E + 06
NQN	0.15E + 09	0.64E + 05
QNS	0.14E + 09	0.65E + 05
QNN	0.13E + 09	0.17E + 06
HNNN	0.17 E + 09	0.37E + 07
ONNNN	0.21E + 09	0.18E + 08

nonradiative decay rates sharply increase due to the decreasing adiabatic excitation energy, while the radiative ones vary slowly, as pointed out previously.[35] However, the radiative decay rates are always much larger than the nonradiative ones in the *X*-annulated rylene derivatives, as a result, the *X*-annulated compounds are expected to be strongly luminescent.

IV. CONCLUSION

To conclude, we have systematically investigated the excited state properties of rylenes and the derivatives in the gas phase, and we proposed a molecular design rule for the red and infrared emission for the elongated rylenes by introducing heteroatom bridges. The semiempirical ZINDO model for calculating the lowest-lying excited states structures is validated by the state-of-the-art CASPT2 method, which reveals that the $1B_u/2A_g$ crossover behavior occurs with respect to the rylene unit length. Most interestingly, we have defined a quantity $\rho_{H/L}$ to characterize the substitution or heteroatom bridges effect on the excited state structure alteration, which is very useful for searching the light-emitting materials by using the simple molecular orbital calculations, without resorting to the complicated and most time-consuming or impossible excited state calculation. The emission spectra, radiative and nonradiative decay rates for a series of *X*-annulated rylene derivatives are predicted, and it is found that they are located at the red and near-infrared range (672, 675, 685, 688, 874, and 1008 nm for NQS, NQN, QNS, QNN, HNNN, and ONNNN, respectively) with large fluorescent quantum yield.

ACKNOWLEDGMENTS

This work is supported by the Ministry of Science and Technology of China (Grant No. 2009CB623600) and the National Science Foundation of China (Grant Nos. 20903102 and 90921007). Professor Z. Y. Wen of Northwest University is deeply acknowledged for his help in MRCI/MNDO calculations.

[1] L. Kuang, Q. Y. Chen, E. H. Sargent, and Z. Y. Wang, J. Am. Chem. Soc. **125**, 13648 (2003).
[2] X. Gong, M. H. Tong, Y. J. Xia, W. Z. Cai, J. S. Moon, Y. Cao, G. Yu, C. L. Shieh, B. Nilsson, and A. J. Heeger, Science **325**, 1665 (2009); G. A. O'Brien, A. J. Quinn, D. A. Tanner, and G. Redmond, Adv. Mater. **18**, 2379 (2006).
[3] S. Gunes, H. S. Neugebauer, and N. S. Sariciftci, Chem. Rev. **107**, 1324 (2007).
[4] S. Kim, Y. T. Lim, E. G. Soltesz, A. M. De Grand, J. Lee, A. Nakayama, J. A. Parker, T. Mihaljevic, R. G. Laurence, D. M. Dor, L. H. Cohn, and M. G. Bawendi, Nat. Biotechnol. **22**, 93 (2004).
[5] A. C. Grimsdale and K. Muellen, Angew. Chem., Int. Ed. **44**, 5592 (2005).
[6] E. Clar, *Polycyclic Hydrocarbons* (Academic, London, 1964), Vol. 2.
[7] J. B. Birks, *Photophysics of Atomatic Molecules* (Wiley, London, 1973).
[8] M. Sonnenschein, A. Amirav, and J. Jortner, J. Phys. Chem. **88**, 4214 (1984).
[9] K. H. Koch and K. Müllen, Chem. Ber. **124**, 2091 (1991).
[10] M. Turki, T. Barisien, J.-Y. Bigot, and C. Daniel, J. Chem. Phys. **112**, 10526 (2000); A. Sugita and T. Kobayashi, Chem. Phys. Lett. **346**, 41 (2001); T. Manaka, T. Yamada, H. Hoshi, K. Ishikawa, and H. Takezoe, Synth. Met. **95**, 155 (1998).
[11] N. J. Turro, *Modern Molecular Photochemistry* (Benjamin/Cummings, California, 1978).
[12] H. L. B. Fang, R. J. Thrash, and G. E. Leroi, J. Chem. Phys. **67**, 3389 (1978); M. F. Granville, G. R. Holtom, and B. E. Kohler, J. Chem. Phys. **72**, 4671 (1980); T. Itoh and B. E. Kohler, J. Phys. Chem. **91**, 1760 (1987).
[13] R. L. Christensen, M. G. I. Galinato, E. F. Chu, J. N. Howard, R. D. Broene, and H. A. Frank, J. Phys. Chem. A **112**, 12629 (2008).
[14] B. S. Hudson and B. E. Kohler, J. Chem. Phys. **59**, 4984 (1973).
[15] K. Schulten, I. Ohmine, and M. Karplus, J. Chem. Phys. **64**, 4422 (1976).
[16] P. Tavan and K. Schulten, J. Chem. Phys. **70**, 5407 (1979); **85**, 6602 (1986); Phys. Rev. B **36**, 4337 (1987).
[17] R. J. Cave, J. Chem. Phys. **92**, 2450 (1990); R. J. Cave and E. R. Davidson, J. Phys. Chem. **91**, 4481 (1987); Chem. Phys. Lett. **148**, 190 (1988).
[18] K. Nakayama, H. Nakano, and K. Hirao, Int. J. Quantum Chem. **66**, 157 (1998).
[19] C.-P. H Hsu, S. Hirata, and M. Head-Gordon, J. Phys. Chem. A **105**, 451 (2001).
[20] L. Serrano-Andres, R. Lindh, B. O. Roos, and M. Merchan, J. Phys. Chem. **97**, 9360 (1993).
[21] J. H. Starcke, M. Wormit, J. Schirmer, and A. Dreuw, Chem. Phys. **329**, 39 (2006).
[22] C. M. Marian and N. Gilka, J. Chem. Theory Comput. **4**, 1501 (2008).
[23] A. R. M. Shahi, C. J. Cramer, and L. Gagliardi, Phys. Chem. Chem. Phys. **11**, 10964 (2009).
[24] A. Shukla and S. Mazumdar, Phys. Rev. Lett. **83**, 3944 (1999).
[25] Z. Shuai, J. L. Brédas, S. K. Pati, and S. Ramasesha, Phys. Rev. B **56**, 9298 (1997).
[26] W. Barford, R. J. Bursill, and M. Y. Lavrentiev, Phys. Rev. B **63**, 195108 (2001).
[27] I. Deperasińska, A. Zehnacker, F. Lahmani, P. Borowicz, and J. Sepioł, J. Phys. Chem. A **111**, 4252 (2007).
[28] S. Karabunarliev, L. Gherghel, K. H. Koch, and M. Baumgarten, Chem. Phys. **189**, 53 (1994); S. Karabunarliev, M. Baumgarten, K. Müllen, and N. Tyutyulkov, Chem. Phys. **179**, 421 (1994).
[29] S. Karabunarliev, M. Baumgarten, and K. Müllen, J. Phys. Chem. A **102**, 7029 (1998).
[30] S. Karabunarliev, M. Baumgarten, E. R. Bittner, and K. Müllen, J. Chem. Phys. **113**, 11372 (2000).
[31] Y. Li and Z. H. Wang, Org. Lett. **11**, 1385 (2009); Y. Li, J. Gao, S. D. Motta, F. Negri, and Z. H. Wang, J. Am. Chem. Soc. **132**, 4208 (2010).
[32] L. P. Chen, X. J. Hou, L. Y. Zhu, S. W. Yin, and Z. Shuai, J. Theor. Comput. Chem. **5**, 391 (2006).
[33] Q. Peng, Y. P. Yi, Z. G. Shuai, and J. S. Shao, J. Chem. Phys. **126**, 114302 (2007); Y. L. Niu, Q. Peng, and Z. G. Shuai, Sci. China, Ser. B: Chem. **51**, 1153 (2008); Q. Peng, Y. L. Niu, C. M. Deng, X. Gao, and Z. Shuai, Chem. Phys. **370**, 215 (2010); Y. L. Niu, Q. Peng, C. M. Deng, X. Gao, and Z. G. Shuai, J. Phys. Chem. A. **114**, 7817 (2010).
[34] Q. Peng, Y. P. Yi, Z. G. Shuai, and J. S. Shao, J. Am. Chem. Soc. **129**, 9333 (2007).
[35] Q. Peng, Y. L. Niu, and Z. G. Shuai, Chem. J. Chin. Iniv. **29**, 2435 (2008).
[36] C. M. Deng, Y. L. Niu, Q. Peng, and Z. Shuai, Acta Phys.-Chim. **26**, 1051 (2010).
[37] A. Dreuw and M. Head-Gordon, Chem. Rev. **105**, 4009 (2005).
[38] G. R. Hutchison, M. A. Ratner, and T. J. Marks, J. Phys. Chem. A **106**, 10596 (2002).
[39] A. D. Becke, J. Chem. Phys. **98**, 1372 (1993).
[40] O. Treutler and R. Ahlrichs, J. Chem. Phys. **102**, 346 (1995); R. Ahlrichs, M. Baer, M. Haeser, H. Horn, and C. Koelmel, Chem. Phys. Lett. **162**, 165 (1989).
[41] M. J. S. Dewar and W. Thiel, J. Am. Chem. Soc. **99**, 4899 (1977).
[42] Y. B. Lei, B. B. Suo, Y. S. Dou, Y. B. Wang, and Z. Y. Wen, J. Comput. Chem. **31**, 1752 (2010).
[43] R. J. Buenker and S. D. Peyerimhoff, Theor. Chim. Acta **35**, 33 (1974); Z. Shuai, D. Beljonne, and J. L. Brédas, J. Chem. Phys. **97**, 1132 (1992); Y. Yi, L. Zhu, and Z. Shuai, J. Chem. Phys. **125**, 164505 (2006).
[44] J. Ridley and M. C. Zerner, Theor. Chim. Acta **32**, 111 (1973).
[45] G. Karlström, R. Lindh, P.-Å. Malmqvist, B. O. Roos, U. Ryde, V. Veryazov, P.-O. Widmark, M. Cossi, B. Schimmelpfennig, P. Neogrady, and L. Seijo, Comput. Mater. Sci. **28**, 222 (2003).
[46] J. Finley, P.-Å. Malmqvist, B. O. Roos, and L. Serrano-Andrés, Chem. Phys. Lett. **288**, 299 (1998).
[47] F. Santoro and B. Dibartolo, *Radiationless Processes* (Plenu, New York, 1980); W. Domcke, D. R. Yarkony, and H. Koppel, *Conical Intersections* (World Scientific, Singapore, 2004).

[48]A. Lami, R. Improta, J. Bloino, and V. Barone, J. Chem. Phys. **128**, 224311 (2008).
[49]Y. He and E. Pollak, J. Phys. Chem. A **105**, 10961 (2001); J. Chem. Phys. **116**, 6088 (2002).
[50]R. Ianconescu and E. Pollak, J. Phys. Chem. A **108**, 7778 (2004); J. Tatchen and E. Pollak, J. Chem. Phys. **128**, 164303 (2008).
[51]A. C. Lasaga, R. J. Aerni, and M. Karplus, J. Chem. Phys. **73**, 5230 (1980).
[52]R. J. Cave, F. Zhang, N. T. Maitra, and K. Burke, Chem. Phys. Lett. **389**, 39 (2004); J. Chem. Phys. **120**, 5932 (2004).
[53]D. Beljonne, Z. Shuai, L. Serrano-Andres, and J. L. Brédas, Chem. Phys. Lett. **279**, 1 (1997).
[54]Z. G. Yu, M. W. Wu, X. S. Rao, X. Sun, and A. R. Bishop, J. Phys.: Condens. Matter **8**, 8847 (1996).
[55]Z. G. Soos, M. H. Hennessy, and G. Wen, Chem. Phys. Lett. **274**, 189 (1997).
[56]B. G. Johnson, P. M. W. Gill, and J. A. Pople, Chem. Phys. Lett. **206**, 239 (1993); F. Furche, J. Chem. Phys. **114**, 5982 (2001); M. J. Frisch, G. W. Trucks, H. B. Schlegel *et al.*, GAUSSIAN 03, Gaussion, Inc., Carnegie, PA, 2003.
[57]C. Joblin, F. Salama, and L. Allamandola, J. Chem. Phys. **110**, 7287 (1999).
[58]X. F. Tan and F. Salma, J. Chem. Phys. **122**, 084318 (2005).
[59]T. M. Halasinski, J. L. Weisman, R. Ruiterkamp, T. J. Lee, F. Salama, and M. Head-Gordon, J. Phys. Chem. A. **107**, 3660 (2003).
[60]B. Fourmann, C. Jouvet, A. Tramer, J. M. Le Bars, and P. Millie, Chem. Phys. **92**, 25 (1985).
[61]M. Rumi, G. Zerbi, K. Müllen, G. Müller, and M. Rehahn, J. Chem. Phys. **106**, 24 (1997).
[62]N. I. Nijegorodov and W. S. Downey, J. Phys. Chem. **98**, 5639 (1994).
[63]I. Deperasińska, B. Kozankiewicz, I. Biktchantaev, and J. Sepioł, J. Phys. Chem. A **105**, 810 (2001).